A&A 413, 1115–1123 (2004)
DOI: 10.1051/0004-6361:20031397

Astronomy & Astrophysics

Comparison of model calculations and photometric observations of bright "magnetic" regions

V. Penza[1,2], B. Caccin[1,3], I. Ermolli[2], and M. Centrone[2]

[1] Dipartimento di Fisica, Università di Roma "Tor Vergata", via della Ricerca Scientifica 1, 00133 Roma, Italia
e-mail: caccin@roma2.infn.it
[2] INAF - Osservatorio astronomico di Roma, via Frascati 33, 00040 Monte Porzio Catone, Italia
e-mail: ilaria@mporzio.astro.it,centrone@mporzio.astro.it
[3] Consorzio Interuniversitario per la Fisica Spaziale (CIFS)

Received 4 june 2003 / Accepted 28 July 2003

Abstract. Since 1981, several attempts to build series of semiempirical models designed to represent, in addition to the quiet Sun, the various types of magnetic regions across the solar disk (network, faculae and sunspots), have followed one another. Here we test the capability of those calculated by Fontenla et al. (1999) to reproduce different experimental data, comparing the computed spectra with the observations made by the PSPT of the Rome Observatory. In particular, we study the average center-limb variation of the network and facular contrast. In this way, we are able to single out the models best reproducing the different photospheric structures operationally identified by the PSPT observations and data analysis. We show also that it would be possible, with slight modifications of the models, to further improve the agreement with the experimental data.

Key words. Sun: atmosphere – Sun: activity – Sun: faculae, plages – Sun: magnetic fields

1. Introduction

Space based measurements of the solar radiation integrated over the entire spectrum (Total Solar Irradiance, TSI) have shown that it varies by about 0.1% over the 11-year magnetic cycle in phase with activity indicators, like the spot numbers or the radio flux. Variations of a few tenths of a percent are recorded over shorter time scales, from days to several months (Fröhlich 2000). These short-term variations are related to the evolution of active magnetic regions, via the combined effect of the appearance of dark (sunspots) and bright (faculae) magnetic features over the solar disk (Hudson et al. 1982; Chapman 1987). On the other hand, the understanding of the mechanisms governing the long term modulation of the TSI by the 11-year activity cycle is less clear and still debated (e.g. Unruh et al. 2000; Li & Sofia 2001).

A major portion of the long term TSI variation is attributed to the changing emission of bright faculae and of the magnetic network (Foukal & Lean 1988; Foukal et al. 1991). However, it has been shown that adjustments of the solar interior induced by variations of internal magnetic fields (Kuhn et al. 1998; Li & Sofia 2001), photospheric temperature changes (Kuhn et al. 1988, 1998) and radius changes (Sofia 1998) may also suitably contribute to these long term irradiance variations.

Since the beginning of 1980s, empirical models have been developed to reconstruct solar irradiance from parameterizations of independently measured proxies of magnetic variability sources, specifically dark sunspots and the bright faculae and network. However, until recently, the understanding of the mechanisms governing TSI variations and their relationship to the solar magnetic field has been fundamentally limited by a lack of spatially resolved, precise solar photometry, together with the absence of contemporary measures of all the solar global parameters. In fact, early work used low-resolution full-disk white light images and mean data archived principally by the NOAA World Data Center to get information about areas, locations and contrasts of sunspots from which to quantitatively determine the net irradiance reduction on a daily basis (Hudson et al. 1982; Sofia et al. 1982; Chapman & Meyer 1986). The analogous approach applied for the estimation of facular and network brightening suffered from great uncertainties in observational determinations of the area, locations and contrasts of these bright magnetic features. These uncertainties were much larger for bright regions than for dark sunspots, so proxies of the facular and network brightening contribution to the TSI were necessarily used. These proxies (for example integrated CaII K flux, MgII index, 10.7 cm radio flux, He 1083 nm equivalent width), based on the observed close correlation between photospheric and chromospheric bright features in faculae and the network, were converted to bolometric brightening, by a careful regression against the observed irradiance adjusted for sunspot darkening (Willson & Hudson 1991; Harvey & Livingston 1994; Fröhlich 1994; De Toma et al. 1997; Fröhlich & Lean 1998). Such

Send offprint requests to: V. Penza,
e-mail: penza@roma2.infn.it

empirical models could account for a large part of the variance in the TSI record (more than 80%), thus suggesting that solar magnetism is the primary cause of TSI variability during the solar cycle. However, none of these models has yet reproduced the entire amplitude and detailed temporal structure of the observed solar irradiance variation. So the identification of the causes of residual TSI variability, which is not explained by these models as an effect of magnetic regions, is still necessary.

Recently, using proxies of facular and network brightening was made unnecessary by the availability of new full-disk photometric observations, daily gathered by a few improved ground-based programs (Johannesson et al. 1998; Chapman et al. 1996; Coulter et al. 1996; Ermolli et al. 1998), as well as by MDI/SOHO (Scherrer et al. 1995).

Parallel, semiempirical atmospheric models representing the various types of active regions across the solar disk have been built and continually improved (Vernazza et al. 1981; Fontenla et al. 1991, 1993, 1999). The combined use of these models with the experimental data about the active regions and their coverage factors permits a more consistent approach with respect to proxies analysis for the understanding of the TSI variations. Actually, some attempts to model the effect of magnetic features on bolometric and spectral variations of the TSI, by using measurements of magnetic region properties through the solar activity cycle have been already presented (e.g. Unruh et al. 2000; Krivova et al. 2003; Caccin & Penza 2003).

2. The RISE models

The latest available series of semiempirical models that try to reproduce the termodynamic structure of the various solar regions (from quiet Sun to faculae, passing through the network, and to sunspots) is that calculated by Fontenla et al. (1999). They are primarily characterized by their temperature structure, determined in such a way as to reproduce particular sets of observations. The procedure used is the following: for a given temperature structure they have solved the equations of statistical equilibrium, radiative transfer for lines and continua and the hydrostatic equilibrium to find the ionization and excitation conditions for each atomic constituent and have calculated the emergent spectrum. By trial and error, they have adjusted the temperature structure so that the emergent spectrum was in best agreement with the observed one (in particular they used the Harvad *Skylab* EUV observations).

Each of the components is treated separately as a plane-parallel one-dimensional atmosphere. Neglecting horizontal interaction between the different components corresponds to considering only surface structures having horizontal dimensions that are larger than the vertical extent of the formation region of the lines and continua studied.

These models were developed with the aim to provide predictions about the behavior of the solar irradiance of the various components of quiet and active regions, also (and mainly) in those spectral ranges that are not observed with sufficient spectral or temporal resolution, and so to permit a better understanding of the variability of the Sun's radiative output. In Fig. 1 the temperature structures are reported (vs. the

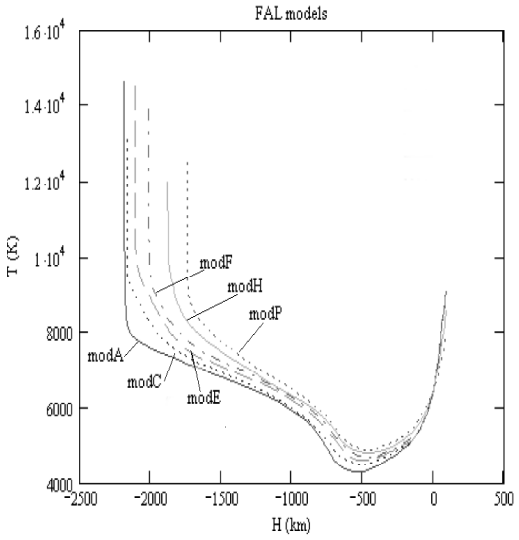

Fig. 1. Temperature structures vs height for six different feature models, which, in order of increasing UV emission, correspond to a faint cell (A), an average cell (C), an average network (E), a bright network or a faint plage (F), an average plage (H) and a bright one (P).

geometrical depth, given in km) for the different features (except the sunspot model, because of its different scale), as in Fontenla et al. (1999).

Fontenla et al. stress that these models do not have an absolute height reference, because the height scale for each model is measured independently of the others.

The authors used different sets of measurements for the construction of the different models and for different parts of them. The photospheric layers are derived from the observed continua in the visible and IR spectrum between 310 nm and 10 μm; the facular models (P and H models) are based in part on the results from Shine & Linsky (1974) and Lemaire et al. (1981) and the temperature structure in their deep layers have been modified relative to quiet Sun models in order to reproduce the center-to-limb variation and facular contrast observed at 1.6 μm by Foukal et al. (1990) and the measurements by Topka et al. (1992, 1997) and Wang et al. (1998). The FAL models have chromospheric layers and a temperature rise, occuring after a temperature minimum, which for all models, except the sunspot model, is located near 500 km above the $\tau_{5000} = 1$ layer. The authors affirm that the determination of this part of the models is less certain of the lower ones, but note that the contribution of these layers to the TSI is less than 5%. Finally, the original models also provide $T(h)$ for the lower and upper transition regions, where many UV and EUV lines are produced, but their contribute to TSI is negligible.

In Fig. 2 there is a comparison between the A and C models (representative of a faint and an average supergranule cell) with Kurucz's model of the Sun (Kurucz 1994).

We want to emphasize that these models are not definitive, because they were constructed to reproduce observations that are far from being complete and are continously updated and improved; moreover, as remarked also by Fontenla et al. (1999), there are not yet physically consistent models that can reproduce *all* the spectral features observed.

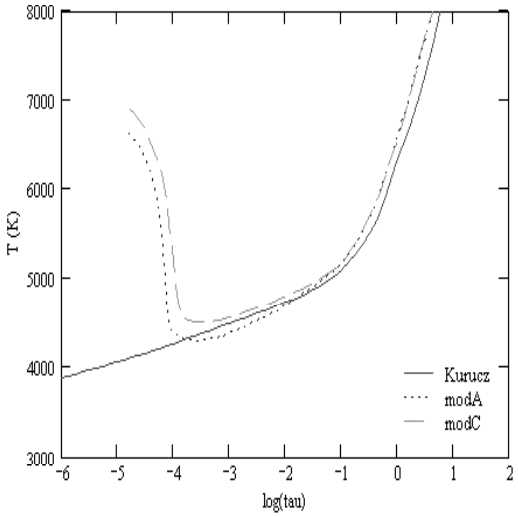

Fig. 2. Comparison of the temperature structures T ($\log(\tau)$) among the models for a faint cell (modA), an averange cell (modC) and Kurucz's model.

Different models are present in the literature, according to the use intended. For example, Unruh et al. (1999, 2000) use models without the temperature rise, taking for the quiet Sun the Kurucz solar model, for the sunspot a model with a $T_{\rm eff}$ of 5150 K interpolated from the Kurucz grids and for the faculae a P model (Fontenla 1993), truncated at about the temperature minimum and extrapolated down to lower temperatures, with a trend similar to Kurucz's. The purpose, in this case, was to mimic, roughly, the behavior of the excitation temperature of most lines in the high photosphere and in the low chromosphere.

3. Spectrum synthesis and photometric data

3.1. Observations

The PSPT is a small (15 cm) refracting telescope optimized to provide high-precision photometric observations by means of a simple optical design minimizing scattered light contamination, an active mirror to reduce tracking errors and a high dynamic range 2048×2048 pixel camera. The PSPT has been developed and constructed by the National Solar Observatory Sacramento Peak in the framework of the NSF-promoted RISE (Radiative Inputs of the Sun to Earth) program, devoted to deepen the understanding of the the 11-yr solar irradiance variations.

Since Rome Observatory joined the program, the first PSPT was installed at Rome in February 1996. The PSPT concept and prototype are described in Coulter & Kuhn (1994) and Ermolli et al. (1998), respectively. The current instrument operation is briefly described by Ermolli et al. (2001), with more complete descriptions available at `http://www.mporzio.astro.it/solare/index.html`.

The results used in this work were obtained by analyzing the archive of daily observations carried out with the PSPT at the Rome Observatory.

In brief, the analyzed images correspond to the observations acquired each day at the three PSPT band-pass centered at CaII K (393.3 ± 0.25 nm) and in the Blue (409.2 ± 0.25 nm) and Red continua (607.1 ± 0.5 nm). These results and the new high-quality measurements of both the photospheric contrast and disk coverage of bright regions on the solar disk since the last solar minimum are presented and discussed by Ermolli et al. (2003a, 2003b).

All the images analyzed were carefully calibrated for instrumental effects (i.e. dark and flat-field corrections), resized in order to get the same disk size, then corrected for the center-to-limb variation of the quiet sun. The latter correction was done by computing the average radial profile of the intensity over the solar disk, excluding active regions from this computation through an intensity threshold criterion.

All the images analyzed were acquired near simultaneously, so no co-alignment among triplet of images is needed.

Facular and network regions were identified on CaII K images by applying automated methods, based on intensity thresholds of contiguous bright regions, described in detail in the paper already cited. We assume the relationship existing between CaII K intensity and magnetic field (Skumanich et al. 1975) to identify the solar features under study on the solar disk. It is under this assumption that, in this paper, we compare measured and synthesized proprieties of "magnetic" bright features. We then assume that continuum and CaII K identified features have essentially identical extent, while we should take into account that corresponding photospheric and chromospheric magnetic features occur at different heights in the solar atmosphere, being cospatial but with a finer structure in the photosphere than their relatively coarse structure in the chromosphere (Chapman & Sheeley 1968).

We defined the feature contrast at each heliocentric position on the disk by the ratio $I_{\rm feature}/I_{\rm quiet}$, where $I_{\rm feature}$ is the photospheric average intensity of the CaII K pixels identified by the automated methods at each heliocentric position and $I_{\rm quiet}$ is the photospheric average intensity of the whole CaII K quiet sun area at the corresponding μ position. The discussion of both the identification methods used and the results obtained with respect to the previous results presented in the literature can be found in Ermolli et al. (2003a, 2003b).

Note that, in the framework of the study presented here, careful analyses of the quality of the images were used, as well as tests of the PSPT telescope characteristics and image calibration accuracy. The main results of these analyses are available at `http://www.mporzio.astro.it/solare/index.html`.

3.2. Spectrum synthesis

By using the FAL models, we are in a position to calculate the emergent intensity for any spectral range in the various active regions and, in particular, the network and facular contrasts and their variation with the heliocentric angle. The comparison of the theoretical results with the experimental data gives us an indication of the capability of these models to reproduce the emergent spectrum and its characteristics.

For the synthesis, we used the SPECTRUM program, written by Gray (2001). It is a stellar spectral synthesis program, written in the C language and distributed with an atomic and

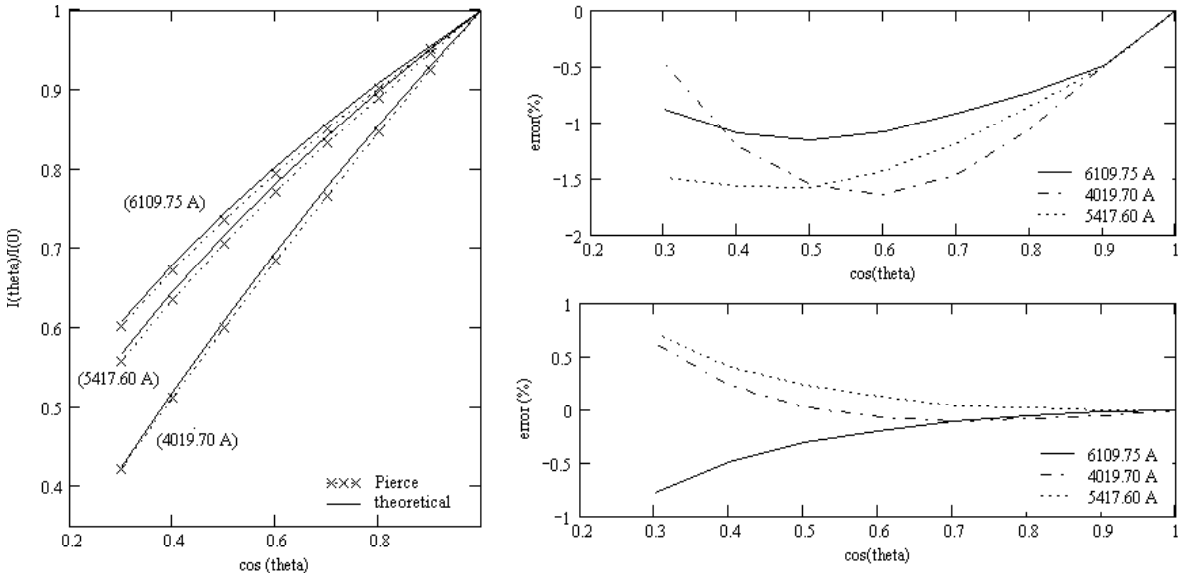

Fig. 3. Left panel: comparison between computed limb darkening $I(\mu)$, for λ = 401.970 nm, λ = 541.760 nm, and λ = 610.975 nm, and the corresponding polynomial representation by Pierce & Slaughter (1977). Right top panel: the percent errors between the reference and computed trend. Right bottom panel: the percent differences between the computed limb darkening from a FAL model with temperature rise (by assuming LTE) relative to that from same model without temperature rise.

molecular line list for the optical spectral region from 300 nm to 680 nm. It uses as input the run of the temperature structure and the electronic density, computing by itself the pressure and the density of the more important species, namely, hydrogen, helium, carbon, nitrogen, oxygen, their ions and the following diatomic molecules: CH, NH, OH, MgH, SiH, CaH, SiO, C2, CN, CO and TiO. Note that SPECTRUM computes synthetic spectra under the LTE assumption and treats each line as a pure absorption line (source function equal to the Planck function). This certainly introduces an error, since the existence of a temperature rise would require a NLTE treatment; the LTE approach, however, does not affect very much the results in the visible range, but only in the UV and EUV. In order to have an idea of the effects of the temperature rise in the LTE approximation, we remade our calculations using models in which the chromospheric temperature increase was replaced by a linear extrapolation of the photospheric relation $\log(T)$ vs. $\log(P)$ or $\log(T)$ vs. $\log(\tau)$, in analogy with Unruh et al. (2000). As a test, we calculated the limb darkening for the monochromatic intensity of the average model at some wavelengths and we compared it with the empirical polynomial representations obtained by Pierce & Slaughter (1977). In Fig. 3 $I(\mu)$, for λ = 401.970 nm, λ = 541.760 nm and λ = 610.975 nm, is reported together with the corresponding errors and the differences between the two different approaches (with or without temperature increase), that at these wavelengths do not exceed 0.5%.

4. Results

4.1. The PSPT bands

Before calculating the intensities for the different models, we analyzed the spectral range in which the PSPT works, testing our capability to reproduce it theoretically, by using, as comparison, an atlas spectrum of the quiet sun (Kurucz et al. 1985). In Fig. 5 we show the result for the blue PSPT band; as it is evident, this zone of the spectrum is very rich in lines and, moreover, it is situated close to the blue wing of the H_δ line. That makes the theoretical signal reproduction more difficult, because the synthesis will strongly depend on line parameters like microturbulence and on the precise wavelength position of the band. On the contrary, as shown in Fig. 4, the red band is much less sensitive to such effects and can be considered a "true" continuum band.

It is interesting to notice that the width of the bands and the presence of lines carries in itself information about photospheric layers different from those that contribute to the continuum formation, as evident from Fig. 6, where we have reported the temperature Response Functions (Caccin et al. 1977), RF_T at constant electronic density for the PSPT bands.

The interpretation of the shape of RF_T is the following: the maximum at $\log(\tau) \approx 0$ corresponds to the continuum formation, that at $\log(\tau) \approx -1.5$ takes into account the formation of the lines that increase their intensity with increasing temperature, while the negative part of RF_T is due to the lines of decreasing intensity with increasing temperature. This is clearer if we analyze the red band, where there are not many lines. In particular, only two lines contribute to the RF_T: Fe I 606.548 nm and Ti I 606.463, whose RF_T are shown in Fig. 7. The reason for the different behavior of the Fe I and Ti I lines derives from the different weight of the derivate of line opacity, χ_L. In fact:

$$\frac{\delta\chi_\mathrm{L}}{\chi_\mathrm{L}} = \frac{\delta\zeta}{\zeta} + \frac{\epsilon_\mathrm{L}}{kT}\frac{\delta T}{T} \quad (1)$$

where ϵ_L is the excitation energy of the lower level and ζ is the ratio of the neutral atom number with respect to the total one, i.e. $\zeta = 1/(1+f)$, where f is given by the Saha

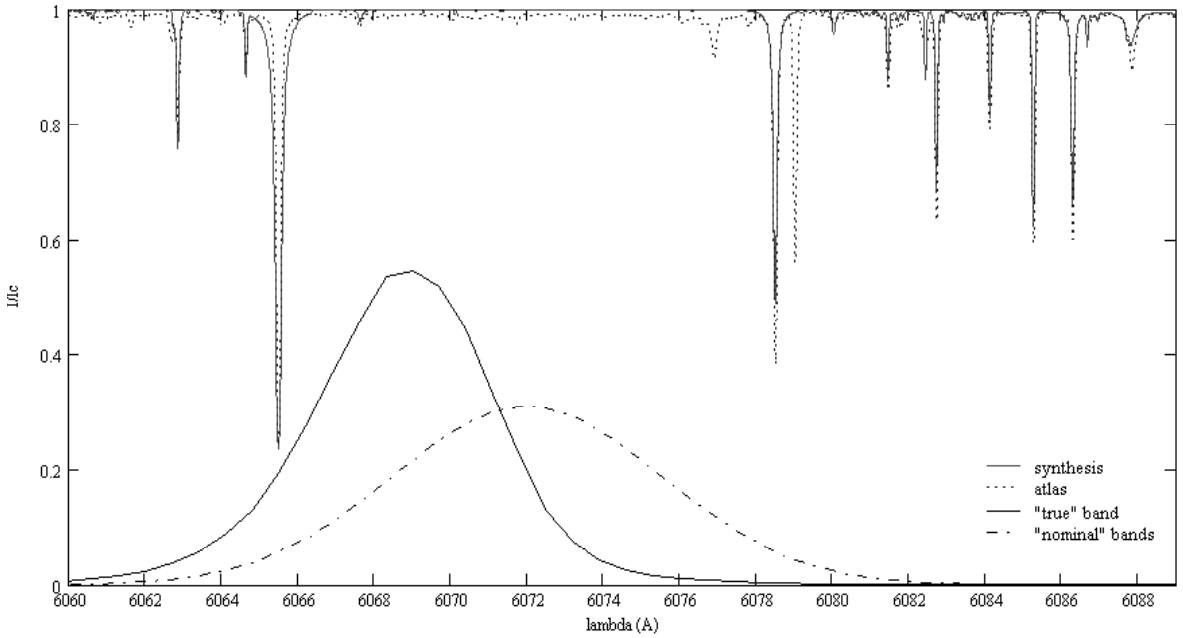

Fig. 4. The PSPT red spectral range: comparison between the theoretically synthesized and that in the Kurucz et al. (1985) Quiet Sun atlas; superimposed the PSPT red band transmission profiles (nominal is for that provided by the filter manufacturer, true is that obtained by the most recent filter calibration).

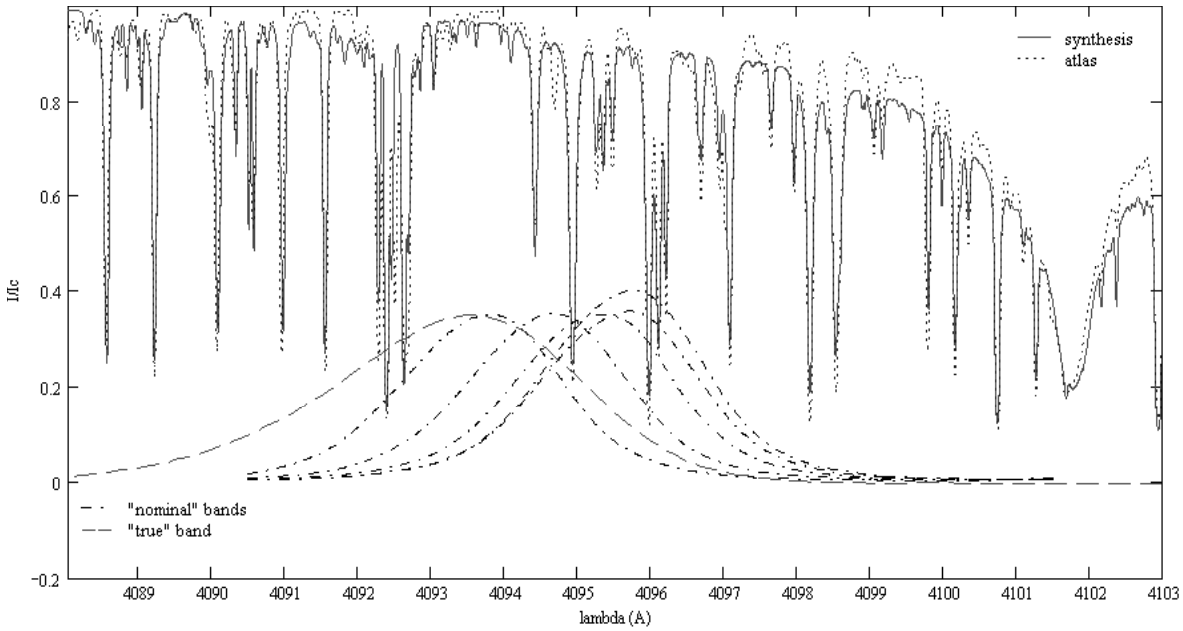

Fig. 5. The PSPT blue spectral range: comparison between the theoretically synthesized and that in the Kurucz et al. (1985) Quiet Sun atlas; superimposed the PSPT blue band transmission profiles (nominal is for that provided by the filter manufacturer at different filter's tilt respect to the optical beam, true is that obtained by the most recent filter calibration).

relation: $f \approx (kT)^{3/2} \exp(-\epsilon_i/kT)$, ϵ_i being the ionization potential. Then, we have

$$\frac{\delta\chi_{\rm L}}{\chi_{\rm L}} \approx -\left(\frac{\epsilon_i}{kT}+\frac{3}{2}\right)\frac{f}{1+f}\frac{\delta T}{T}+\frac{\epsilon_{\rm L}}{kT}\frac{\delta T}{T}$$
$$\approx \frac{(1+f)\epsilon_{\rm L}-f\epsilon_i}{1+f}\frac{1}{kT}\frac{\delta T}{T}.$$

For the Ti line, this term (negative in both cases) is much larger than for the Fe one and determines the sign of $RF_{\rm T}$.

4.2. The network and facular contrast

In order to show how much the blue contrast is a very "delicate" observable, we report in Fig. 8 the different computed contrasts between modE (representative of the network) and modC (used as representative of the quiet Sun) obtained with different pass-bands (for simplicity sake we used Gaussians of the form $G(\lambda) = \exp(\lambda - \lambda_0)^2/\sigma^2$), with values of σ between 0.05 and 0.25 nm and λ_0 equal, in turn, to 409.60 nm and 409.38 nm) and in Fig. 9 those for different microturbulence parameters.

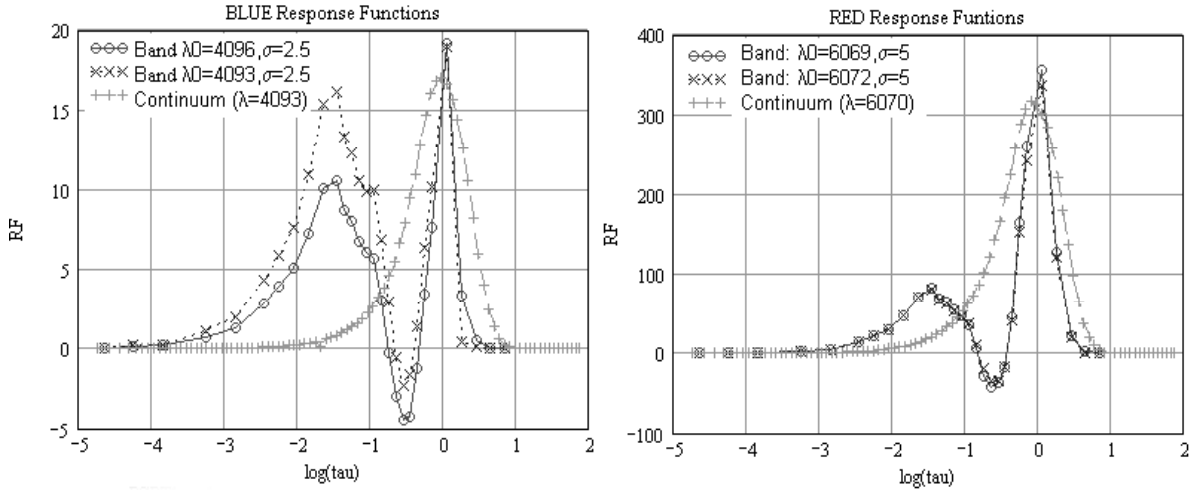

Fig. 6. Temperature Response Functions (at N_e constant) versus $\log(\tau)$ (τ is the contiuum optical depth at 500 nm) for the blue (left) and the red (right) band, obtained using different telescope transmission filters. Superimposed there are those calculated for the only continuum.

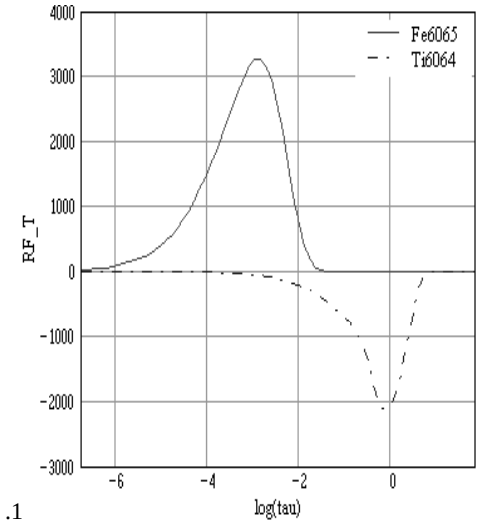

Fig. 7. Temperature Response Function (at N_e constant) versus $\log(\tau)$ (τ is the continuum optical depth at 500 nm) for the two lines FeI 606.548 nm and TiI 606.463 nm. The units are arbitral.

We have made an analogous check for the modH (representative of average faculae) contrast, which, however, seems to be less affected by the variation of these parameters (passing from $\xi_H = 1$ to $\xi_H = 1.4$ the contrast changes only by 0.2%); moreover, because the facular contrast is higher than the network one, this effect results less important. We stress that the microturbulence parameter that we enter in the spectral synthesis should be consistent with the microturbulence of the model (varying from 0.3 to 2 km s^{-1}); indeed, the magnitude of the microturbulence affects the line opacity, which affects the structure of the stellar atmosphere. However, minor departures from the model microturbulence do not represent a severe inconsistency (for instance Kurucz, in his grids (Kurucz 1994), uses 1.0 km s^{-1} in the computation of the synthetic spectrum of the Sun, even though his solar model was computed with a microturbulent velocity of 1.5 km s^{-1}).

The sensitivity of the blue contrast to the pass-band parameters derived from our calculations were quite significant within the "nominal" range, provided by the PSPT constructors (Figs. 5 and 4); therefore a detailed instrumental calibration was needed. The results presented in the following are obtained by using the carefully recalibrated trasmission profile of the filters used at the Rome PSPT (Centrone et al. 2002).

In Figs. 10 and 11 the comparison between theoretical results and experimental PSPT data for the network (theoretically represented by modE) and for the faculae (theoretically represented by modF and modH) contrast is shown, while the numerical data of the computed intensities for all of the models are reported in Tables 1 and 2 (for the blue band we report only those providing a better agreement with the experimental data, i.e. with ξ_E, ξ_F and $\xi_H = 1.4$ km s^{-1}). We have calculated these values both with the "original" FAL models and with the models without chromospheric temperature rise, obtaining no substantial difference.

Figure 10 shows that a very good agreement is reached for the network contrast, provided that we take into account the following geometrical effect: because the network is a very thin feature, its measurement can be "polluted" by the quiet Sun in a way that depends on the sight line direction (i.e. on the heliocentric angle). We can do the following two-dimensional estimate: suppose that the network contribution to the emergent intensity is assimilable to a Dirac delta:

$$I = I_q[1 - \delta(x)] + I_n\delta(x) \tag{2}$$

where I_q and I_n are quiet and network intensity at "infinite resolution". This intensity must be, first of all, convolved with a (normalized) instrumental profile (that takes into account both the finite instrumental resolution and the seeing effects) $\phi(x)$ and then averaged over an interval Δx.

At the disk center, we have:

$$I = I_q + (I_n - I_q)\int_{-\infty}^{+\infty}\phi(x')\delta(x' - x)\mathrm{d}x' = I_q + (I_n - I_q)\phi(x)$$

and, by averaging:

$$I^{av} = I_q + (I_n - I_q)\frac{1}{2\Delta x}\int_{-\Delta x}^{\Delta x}\phi(x)\mathrm{d}x \approx I_n. \tag{3}$$

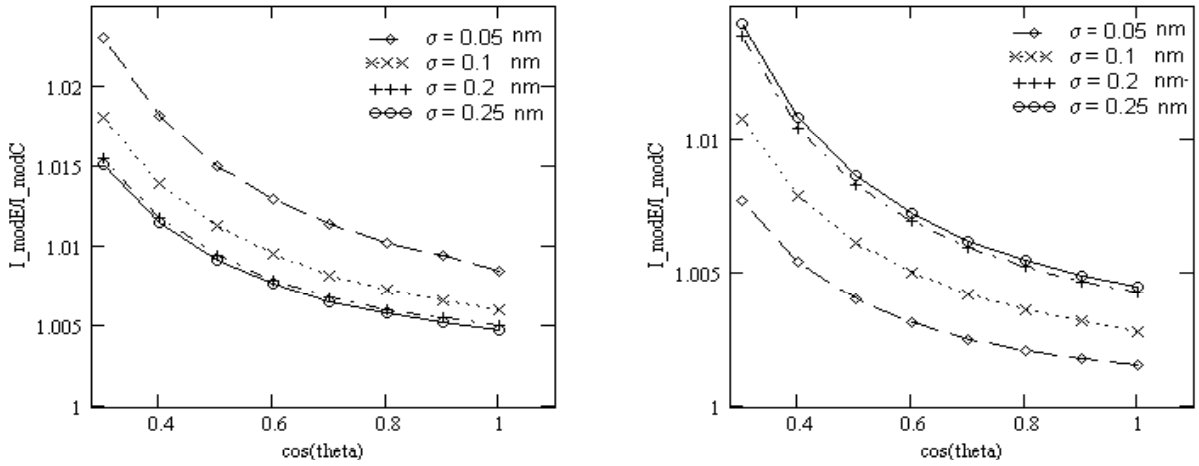

Fig. 8. The contrast between ModE and ModC for different pass-bands, taken as Gaussians centered at two different wavelengths (left: λ_0 = 409.60 nm, right: λ_0 = 409.38) and with Gaussian variances (σ) between 0.05 and 0.25 nm. For all cases, the microturbulence is fixed at ξ = 1 km s^{-1}.

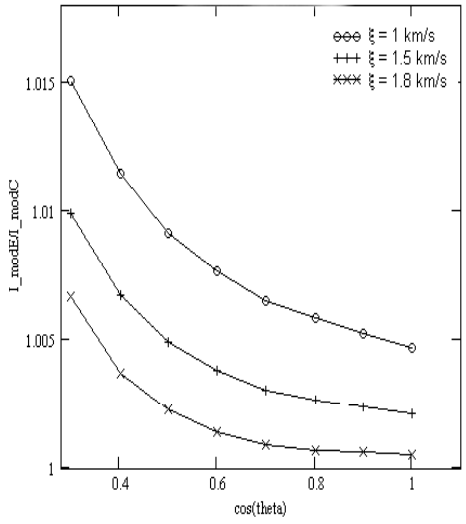

Fig. 9. The contrast between ModE and ModC for different microturbulence parameters (ξ), with a Gaussian pass-band centered at λ_0 = 409.60 nm and with σ = 0.25 nm.

Instead, for $\mu \neq 1$, the first effect will be a stretching of $\phi(x)$:

$$I = I_{\rm q} + (I_{\rm n} - I_{\rm q}) \int_{-\infty}^{+\infty} \phi(x'/\mu)\delta(x' - x)\mathrm{d}x' = I_{\rm q} + (I_{\rm n} - I_{\rm q})\phi(x/\mu).$$

Then also Δx will suffer the same phenomenon:

$$I^{\rm av} = I_{\rm q} + (I_{\rm n} - I_{\rm q})\frac{1}{2\Delta x/\mu} \int_{-\Delta x/\mu}^{\Delta x/\mu} \phi(x/\mu)\mathrm{d}x \approx I_{\rm q}(1-\mu) + \mu I_{\rm n}.$$

This dilution effect does not affect very much the facular contrast, the faculae being more extensive structures than network. Figure 11 shows the good agreement between modF synthesis and the experimental data.

However, a careful analysis of Fig. 11 and of Tables 1 and 2 reveals the presence of a negative contrast at the center of the disk for modP (both in the red and in the blue band) and for modH (only in the red band). This behavior does not have an experimental verification in the PSPT data and is due to the particular photospheric temperature structure of the P and H models, that is colder than the average Sun. Fontenla et al. (1999) affirm to have intentionally modified such models in this way in order to reproduce the center-to-limb variation and facular contrast measured at 1.6 μm (Foukal et al. 1990; Topka et al. 1992; Wang et al. 1998), that shows a negative contrast. Actually, as discussed by Foukal & Moran (1994), Sobotka et al. (2000) and Sanchez et al. (2002), faculae and pores seem to share the same physical mechanism (lateral heating and inhibition of

Table 1. The emergent intensity integrated over the red PSPT band, calculated with the six different FAL models. The intensity unit is 10^6 erg s^{-1} cm^{-2} sr^{-1}.

cos(θ)	ModA	ModC	ModE	ModF	ModH	ModP
1	9.696	9.705	9.713	9.729	9.698	9.642
0.9	9.262	9.272	9.282	9.301	9.330	9.334
0.8	8.772	8.784	8.796	8.820	8.916	9.007
0.7	8.304	8.292	8.305	8.334	8.496	8.651
0.6	7.771	7.784	7.800	7.835	8.063	8.258
0.5	7.189	7.208	7.227	7.272	7.570	7.837
0.4	6.535	6.574	6.596	6.655	7.025	7.360
0.3	5.824	5.856	5.880	5.978	6.411	6.805

Table 2. The emergent intensity integrated over the blue PSPT band, calculated with the six FAL models. The intensity unit is 10^5 erg s^{-1} cm^{-2} sr^{-1}.

cos(θ)	ModA	ModC	ModE	ModF	ModH	ModP
1	5.066	5.092	5.099	5.151	5.132	5.059
0.9	4.734	4.761	4.768	4.821	4.844	4.816
0.8	4.382	4.410	4.417	4.473	4.538	4.557
0.7	4.008	4.016	4.025	4.103	4.213	4.279
0.6	3.610	3.640	3.650	3.710	3.866	3.981
0.5	3.187	3.217	3.230	3.293	3.493	3.658
0.4	2.735	2.778	2.784	2.851	3.091	3.303
0.3	2.253	2.291	2.312	2.384	2.658	2.908

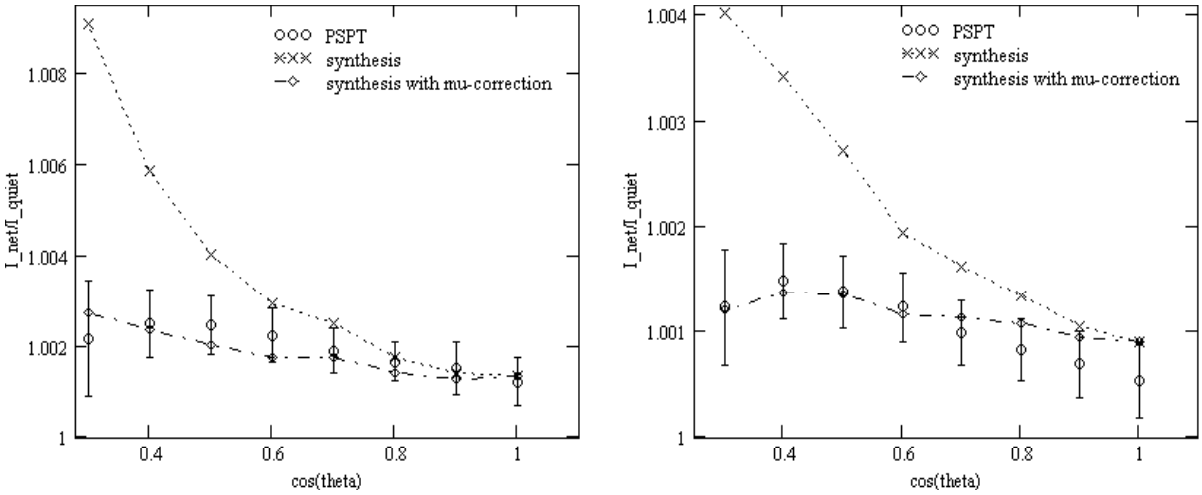

Fig. 10. The network contrast (modE/modC), with microturbulence $\xi_E = 1.4$ km s^{-1}, calculated in the calibrated PSPT pass-bands, comparated with the results of PSPT data analysis (Right: blue contrast, left: red contrast).

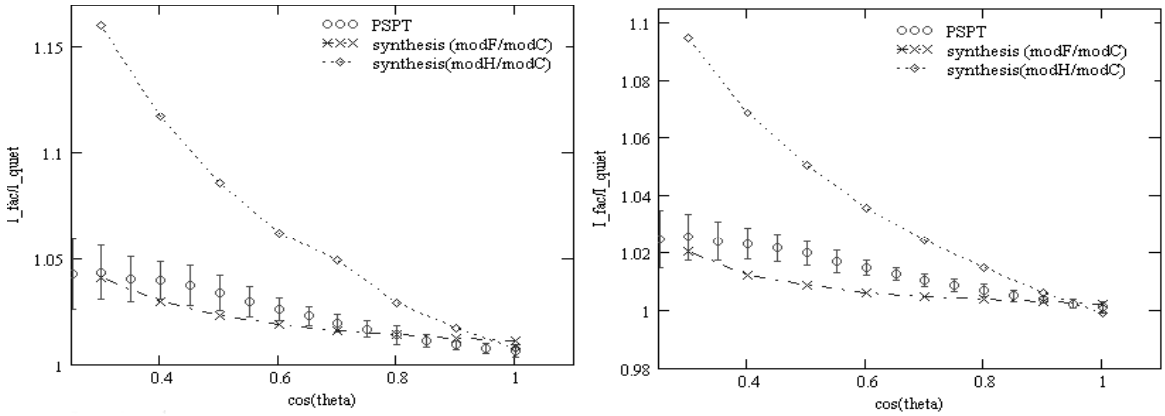

Fig. 11. Comparison between the synthetized facular contrast (modF and modH over modC), calculated in the calibrated PSPT pass-bands, and the results of PSPT data analysis (Right: blue contrast, left: red contrast).

convection), which simply changes its contribution as a fuction of the size of the structure. So structures presenting negative contrast both at 1.6 μm and in the visible range should be defined, more correctly, as a pore.

We have reason to believe that, above all in the blue band, the phenomenon of the dark faculae, obtained in our synthesis, is the not desired consequence of an excessive cooling of the modH and modP photospheres. Our study has the aims to provide indications about the models of *bright* structures in order to use them, subsequently, in the reconstruction of the irradiance variations.

We show that it is possible to slightly modify these models, increasing the slope of the temperature structure in the photospheric zone by an amount sufficient to make the contrast positive in the visible, but negative at 1.6 μm, near the disk center, at least for modP. The modifications brought to the temperature structures are shown in Fig. 12.

We must recall, hovewer, that we cannot test the real goodness of the H and P models (modifed or not), because we have already seen that they are too bright to be representive of an average behavior, as that provided by the PSPT data used in this study.

5. Conclusions

We have tested the capability of the FAL models to reproduce experimental data that were different from those on which these semiempirical models were based. The final goal is that of providing average models that can be used to evaluate the contribution to solar irradiance variations of different bright features. In particular, we have compared "theoretical" results, derived by the spectral synthesis of these semiempirical models, with PSPT photometric data corresponding to the center-limb trend of network and facular contrast. Through this comparison, we could determine that modE is the model best reproducing the behavior of the network (the difference between the experimental contrast and computed one is less than 0.05% until $\mu \approx 0.3$). It was necessary, however, to consider a dilution effect of the network with the quiet photosphere, due to thinness of the first one and to geometrical effects.

The facular contrast, instead, is well identified by modF (with an error less than 1%). We have noted that the network blue contrast is very sensitive both to the parameters of the band-pass and to the microturbulence. This sensitivity, instead, does not play an important role in the facular contrast

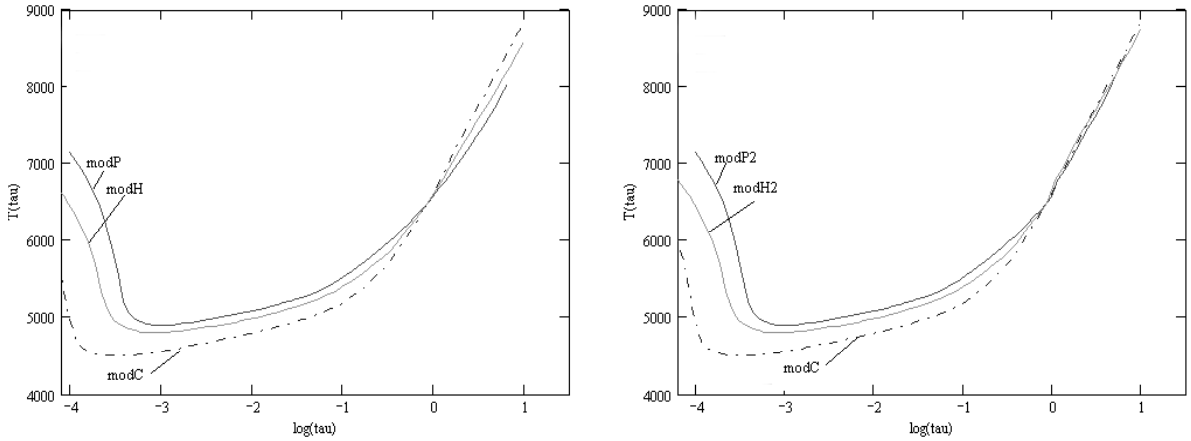

Fig. 12. Left panel: temperature structures of modH and modP with respect to that of modC; right panel: the modH and modP modified in their photospheric zone (indicated with modP2 and modH2).

computation or in the red band (where a very minor number of lines are present with respect to the blue band).

Finally, we have shown that it is possible to slightly modify the models in order to optimize some details of the comparison (e.g. to obtain a positive contrast at the disk center). We note, however, that the correspondence between models and structures, and the necessity of suitable modifications, depends upon the details of the data acquisition and elaboration, that operationally define the proprieties of the observed magnetic structures. Where other data (or other methods) were used, other modifications or other models could be required.

Acknowledgements. The authors thank M. T. Gomez for useful model checks.

References

Caccin, B., Gomez, M. T., Marmolino, C., & Severino, G. 1977, A&A, 54, 227
Caccin, B., & Penza, V. 2003, Mem. SAIt, in press
Centrone, M., Giorgi, F., & Ermolli, I. 2002, Technical Report Rome Observatory, 02-S2
Chapman, G. A., & Sheeley, N. R., Jr 1968, Sol. Phys., 5, 442
Chapman, G. A., & Meyer, A. D. 1986, Sol. Phys., 103, 21
Chapman, G. A. 1987, ARA&A, 25, 633
Chapman, G. A., Cookson, A. M., & Dobias, J. J. 1996, J. Geophys. Res., 101, 13541
Coulter, R. L., & Kuhn, J. R. 1994, ASP Conf. Ser., 68, 37
Coulter, R. L., Kuhn, J. R., & Lin, H. 1996, AAS, 188, 5604
de Toma, G., White, O. R., Knapp, B. G., Rottman, G. J., & Woods, T. N. 1997, J. Geophys. Res., 102, 2597
Ermolli, I., Fofi, M., Bernacchia, C., et al. 1998, Sol. Phys., 177, 1
Ermolli, I., Centrone, M., & Fofi, M. 2001, Mem. SAIt, 72, 673
Ermolli, I., Berrilli, F., & Florio, A. 2003a, in press
Ermolli, I., Centrone, M., & Criscuoli, S. 2003b, in preparation
Fontenla, J., Avrett, E. H., & Loeser, R. 1991, ApJ, 377, 712
Fontenla, J., Avrett, E .H., & Loeser, R. 1993, ApJ, 406, 319
Fontenla, J., White, O. R., Fox, A. P., Avrett, E. H., & Kurucz, R. L. 1999, ApJ, 518, 480
Foukal, P., & Lean, J. 1988, ApJ, 328, 347
Foukal, P., Little, R., Graves, J., Rabin, D., & Lynch, D. 1990, ApJ, 353, 712
Foukal, P., Harvey, K., & Hill, F. 1991, ApJ, 383, L89
Foukal, P., & Moran, T. 1994, in Infrared Solar Physics, ed. D. Rabin, J. T. Jefferies, & C. Lindsey, IAU Symp., 154, 23
Fröhlich, C. 1994, in The Sun as a Variable Star, ed. J. M. Pap, C. Frölich, H. S. Hudson, & S. K. Solanki, IAU Symp., 143, 28
Fröhlich, C., & Lean, J. 1998, Geophys. Res. Lett., 25, 4377
Fröhlich, C. 2000, Space Sci. Rev., 94, 15
Gray, R. 0. 2001, `http://www.phys.appstate.edu/spectrum/spectrum.html`
Johannesson, A., Marquette, W. H., & Zirin, H. 1998, Sol. Phys., 177, 265
Harvey, J. W., & Livingston, W. C. 1994, in Infrared Solar Physics, ed. D. Rabin, J. T. Jefferies, & C. Lindsey, IAU Symp., 154, 59
Hudson, H. S., Silva, S., Woodard, M., Willson, R. C., & Gorlova, N. I. 1982, Sol. Phys., 76, 211
Krivova, N. A., Solanki, S. K., Fligge, M., & Unruh, Y. C. 2003, A&A, 399, L1
Kuhn, J. R., Libbrecht, K. G., & Dicke, R. H. 1988, Science, 242, 908
Kuhn, J. R., Bush, R. I., Scherrer, P., & Scheick, X. 1998, Nature, 392, 155
Kurucz, R. L., Furenlid, I., Branult, J., & Testerman, L. 1985, Sky and Telescope, 70, 38
Kurucz, R. L. 1994, CD-ROM No. 19
Lemaire, P., Goutterbroze, P., Vial, J. C., & Artzner, G. E. 1981, A&A, 103, 160
Li, L. H., & Sofia, S. 2001, ApJ, 549, 1204
Pierce, A. K., & Slaughter, C. D. 1977, Sol. Phys., 51, 25
Sánchez, C. M., Vázquez, M., Bonet, J. A., & Sobotka, M. 2003, ApJ, 570, 886
Scherrer, P. H., Bogar, R. S., & Bush, R. I. 1995, Sol. Phys., 162, 129
Shine, R. A., & Linsky, J. L. 1974, Sol. Phys., 39, 49
Skumanich, A., Smythe, C., & Frazier, E. N. 1975, ApJ, 200, 747
Sobotka, M., Vàzquez, M., Sánchez Cuberes, M., Bonet, J. A., & Hanslmeier, A. 2000, ApJ, 544, 1155
Sofia, S., Oster, L., & Schatten, K. 1982, Sol. Phys., 80, 87
Sofia, S. 1998, Mem. SAIt, 69, 531
Topka, K. P., Tarbell, T. D., & Title, A. M. 1992, ApJ, 396, 351
Topka, K. P., Tarbell, T. D., & Title, A. M. 1997, ApJ, 484, 479
Unruh, Y. C., Solanki, S. K., & Fligge, M. 1999, A&A, 345, 635
Unruh, Y. C., Solanki, S. K., & Fligge, M. 2000, Space Sci. Rev., 94, 145
Vernazza, J. E., Avrett, E. H., & Loeser, R. 1981, ApJS, 45, 635
Wang, H., Spirock, T., Goode, P. R., et al. 1998, ApJ, 495, 957
Willson, R. C., & Hudson, H. S. 1991, Nature, 351, 42